Numerical Modelling and Design of LiteSteel Beams Subject to Lateral Buckling

T. Anapayan and M. Mahendran
Faculty of Built Environment and Engineering
Queensland University of Technology, Brisbane, QLD 4000, Australia

Abstract: The LiteSteel Beam (LSB) is a new hollow flange channel section developed using a patented dual electric resistance welding and cold-forming process. It has a unique geometry consisting of torsionally rigid rectangular hollow flanges and a slender web, and is commonly used as flexural members. However, the LSB flexural members are subjected to a relatively new lateral distortional buckling mode, which reduces their moment capacities. Unlike lateral torsional buckling, the lateral distortional buckling of LSBs is characterised by simultaneous lateral deflection, twist and cross sectional change due to web distortion. Therefore a detailed investigation into the lateral buckling behaviour of LSB flexural members was undertaken using experiments and finite element analyses. This paper presents the details of suitable finite element models developed to simulate the behaviour and capacity of LSB flexural members subject to lateral buckling. The models included all significant effects that influence the ultimate moment capacities of such members, including material inelasticity, lateral distortional buckling deformations, web distortion, residual stresses, and geometric imperfections. Comparison of elastic buckling and ultimate moment capacity results with predictions from other numerical analyses and available buckling moment equations, and experimental results showed that the developed finite element models accurately predict the behaviour and moment capacities of LSBs. The validated model was then used in a detailed parametric study that produced accurate moment capacity data for all the LSB sections and improved design rules for LSB flexural members subject to lateral distortional buckling.

Keywords: *LiteSteel beam, Flexural members, Lateral distortional buckling, Numerical modelling, Cold-formed steel structures, Hollow flanges, Slender web.*

1. Introduction

In recent times, the use of cold-formed steel members in the building industry has increased considerably due to the availability of advanced roll-forming technologies and thin and high strength steels. Although cold-formed steel members are considered to be more cost efficient than hot-rolled steel members, they suffer from many complex buckling modes and their interactions because they are usually slender and unsymmetric sections. Therefore an advanced cold-formed steel section, called the LiteSteel Beam (LSB), was introduced by OneSteel Australian Tube Mills (OATM) to replace the conventional cold-formed C- and Z-sections and smaller hot-rolled I- and channel sections. The new LSB sections shown in Figure 1 are made of two torsionally rigid closed flanges and a slender web from a single strip of steel using OATM's patented dual electric resistance welding and automated continuous roll-forming process. Their unique geometry and light weight make them more efficient than hot-rolled steel members. Table 1 shows the currently available LSB sections and their dimensions [1]. The high strength steel used for LSB sections is DuoSteel grade with web and flange yield stresses of 380 and 450 MPa, respectively. The higher flange yield stress is the result of the cold-forming process used in making LSBs.

The LSBs have found increasing popularity in residential, industrial and commercial buildings as flexural members such as bearers and joists. The LSB is considered to be on average 40% lighter than traditional hot-rolled steel beams of equivalent performance [1]. When LSBs are used as flexural members, they are subjected to a relatively new Lateral Distortional Buckling mode, which reduces their member moment capacities, particularly for intermediate spans. Unlike the commonly observed lateral torsional buckling of steel beams, the lateral distortional buckling of LSBs is characterised by simultaneous lateral deflection, twist and cross sectional change due to web distortion as shown in Figure 2.

Elastic lateral buckling of channel section beams has been investigated and summarised in many books [2-4]. In comparison, studies on the lateral distortional buckling behaviour of beams are limited. Effects of lateral distortional buckling on the behaviour of conventional I-sections were first investigated by Hancock et al. [5] and Bradford [6]. Elastic lateral distortional buckling and ultimate strength behaviour of a doubly symmetric HFB with triangular hollow flanges, known as hollow flange beams (HFB), was investigated using numerical analyses and experiments as described in [7-9]. A study on the use of web

stiffeners to eliminate lateral distortional buckling of HFBs is described in [10,11]. Pi and Trahair [12] also investigated the lateral distortional behaviour of HFBs using a nonlinear inelastic analysis method. However, the ultimate strength behaviour of the new mono-symmetric LSB flexural members subject to lateral distortional buckling has not been investigated. Effects of mono-symmetric cross-section, web distortion, initial geometric imperfections, residual stresses and stress-strain characteristics on the lateral distortional behaviour of LSBs are not known. Therefore an experimental study was first conducted to investigate the lateral distortional buckling behaviour of LSB flexural members. Details of the experimental study and its results are presented in [13]. This was followed by a numerical study to develop validated finite element models of LSBs, which were then used in a detailed parametric study to develop moment capacity curves and improved lateral distortional buckling design rules for LSBs.

This paper presents a description of the developed finite element models of LSB flexural members, capable of simulating the significant behavioural effects of material inelasticity, buckling deformations including web distortion, residual stresses and geometric imperfections. The results from both elastic buckling and non-linear static analyses of LSBs were compared with corresponding results from finite strip analyses and experimental results reported in [13]. It includes the details of the parametric study undertaken using the validated finite element models and the improved lateral distortional buckling design rules for LSBs.

2. Finite Element Model Description

Two types of finite element models were considered to simulate the behaviour of LSB flexural members, referred to as the ideal and experimental finite element models in this paper. They are described next.

- Ideal finite element models (Figure 3a) – These models incorporated ideal conditions such as idealised simply supported boundary conditions and a uniform bending moment, nominal dimensions, yield stresses, geometric imperfections and residual stresses. These idealised conditions simulated the worst case, and hence they were used in the parametric study to develop moment capacity design curves.
- Experimental finite element models (Figure 3b) – These models were developed to simulate the actual test members' physical geometry, loads, constraints, mechanical

properties, geometric imperfections and residual stresses as closely as possible. They were used in the comparison with experimental test results of LSBs subjected to quarter point loads presented in [13]. This comparison was intended to establish the validity of the finite element model for explicit modelling of initial geometric imperfections, residual stresses, lateral distortional buckling deformations, and associated material yielding in non-linear static analyses. Although this does not directly verify the suitability of the ideal finite element model for the development of moment capacity curves, this approach is acceptable as the ideal conditions are based on theoretical assumptions and are difficult to simulate in real experiments.

The ideal model was based on the nominal dimensions and thicknesses of LSBs given in Table 1 whereas the experimental model was based on the measured values reported in [13]. Both ideal and experimental finite element models did not consider the rounded corners although the LSB sections have such corners as shown in Table 1 and Figure 1. The LSB sections have an inner radius of 3 mm at the web-flange junction while the outer radius is equal to twice the thickness.

In order to determine the level of approximations involved in using LSB sections without rounded corners in finite element analyses (FEA), the cross-sectional properties of LSBs and their elastic lateral distortional buckling moments for spans from 1.5 to 10 m were evaluated using rounded and right angle corners. Elastic section moduli of the 13 LSB sections were calculated using a well established finite strip analysis program, Thin-Wall, and the results (Table 1) showed that the idealised LSBs with right angle corners over-estimated the elastic section modulus by 2.79% on average (varied from 2.25 to 3.60%). Elastic lateral distortional buckling moment results showed that the use of idealised LSB section with right angle corners led to an over-estimation by 2.6% on average. The difference varied from 1.7% for long spans to 4.9% for short spans [14]. Based on these results, it can be concluded that the effect of including rounded corners is small and that it is adequate to use the idealised LSB with right angle corners in FEA. Effects of rounded corners on other section properties of LSBs were also small. Most importantly, since the FEA moment capacity results of idealised LSB sections will be non-dimensionalised in the development of design rules, such small differences in section properties and elastic buckling moment capacities with the use of idealised LSBs will not influence the final design rules or recommendations of this research.

Both ideal and experimental finite element models were developed using MD R2.1/ PATRAN pre-processing facilities while they were analysed using ABAQUS [15]. MD R2.1/PATRAN post-processing facilities were then used to view the results from the ABAQUS analyses.

2.1 Discretization of the Finite Element Mesh

Shell elements are generally used to model thin-walled structures. ABAQUS [15] includes general purpose shell elements, which provide robust and accurate solutions in most applications and have the capability of providing sufficient degrees of freedom. Therefore local buckling deformations and spread of plasticity could be explicitly modelled. The shell element in ABAQUS [15] called S4R5 was used to develop the LSB model. This element is thin, shear flexible, isometric quadrilateral shell with four nodes and five degrees of freedom per node, utilizing reduced integration and bilinear interpolation scheme.

Finer meshes are generally preferred to obtain accurate predictions although there are no general guidelines on the required mesh density, which depends on the type of structure and analysis [16]. But finer meshes make the process more expensive in terms of computational time and resources. A convergence study showed that a minimum mesh size density comprising of 5 mm × 10 mm elements was required to represent accurate residual stress distributions, spread of plasticity, and local buckling deformations of LSBs. Element widths equal to or less than 5 mm and a length of 10 mm were selected as the suitable mesh size as shown in Figure 4. Nine integration points through the thickness of the elements were used to model the distribution of flexural residual stresses in the LSB sections and the spread of plasticity through the thickness of the shell elements. Kurniawan and Mahendran [17] also used the same mesh size and the number of integration points in their models of LSBs to investigate the effects of moment distribution and load height on moment capacity.

2.2 Material Model and Properties

The ABAQUS classical metal plasticity model was used in the analysis. This model implements the von Mises yield surface to define isotropic yielding, and associated plastic flow theory. The ideal models included the nominal web and flange yield stresses of 380 and 450 MPa, respectively. These yield stresses are the minimum specified values for the range of

LSB sections. The yield stresses of web, inside and outside flanges were also measured using tensile coupon tests as reported in [13], and these measured yield stresses shown in Table 4 were used in the experimental models of LSBs.

A perfect plasticity model based on simplified bilinear stress-strain curve with no strain hardening was used for all the models. Isotropic hardening model that allows strain hardening behaviour where yield stresses increase as plastic strain occurs was not considered. This may be important when modelling sections subjected to localised yielding involving strain hardening effects. However, since all the beams modelled here were mainly subjected to lateral buckling effects, a simple elastic perfect plastic model was assumed to be accurate. The elastic modulus E and Poisson's ratio v were taken as 200,000 MPa and 0.3, respectively, for both the ideal and experimental finite element models.

2.3 Load and Boundary Conditions

The loads and boundary conditions of the ideal and experimental finite element models have similarities and contrasts. They are described separately in the following sections.

2.3.1 Ideal Finite Element Model

"Idealised" simply supported boundary conditions with a uniform bending moment were considered to be the critical case for the development of moment capacity design rules. Therefore the ideal finite element model of LSBs considered the "Idealised" simply supported boundary conditions based on the following requirements [3,18].

1. Simply supported in-plane - Both ends fixed against in-plane vertical deflection but unrestrained against in-plane rotation, and one end fixed against longitudinal horizontal displacement.
2. Simply supported out-of-plane - Both ends fixed against out-of-plane horizontal deflection, and twist rotation, but unrestrained against minor axis rotation and warping displacements of flanges.

Figure 5 shows the above boundary conditions used in the ideal finite element model considered here. The presence of symmetry allowed the use of only half the span. The global axes selected to input the boundary conditions for the analysis are also shown in Figure 5. The ideal simply supported boundary condition at one end was modelled by using a Single Point

Constraint (SPC) of "234" applied to all the nodes at the end, ie. y and z translations and x-axis rotation are restrained. Symmetrical boundary condition of SPC "156" was applied to the mid-span of LSB.

To simulate a uniform end moment across the section, linear forces were applied at every node of the beam end, where the nodes above the middle of the web were subject to tensile forces while the nodes below the middle of the web were subject to compressive forces. The force at the middle of the web was zero and was linearly increased within the cross section as shown in Figure 6. A tensile force of 1000 N and a compressive force of 1000 N were applied at the nodes on the top and bottom faces of LSB cross section. Figure 6 shows the applied loads on each node of a 200x45x1.6 LSB section. The simulated moment due to the applied loads at each node can be calculated by multiplying the load at each node by the distance of the corresponding node to the middle of the web. The total moment is the arithmetic sum of the above individual moments.

2.3.2 Experimental Finite Element Model

In the experimental study of LSBs [13], a quarter point loading was applied at the shear centre of LSBs with the "Idealised" simply supported boundary conditions as mentioned in the previous section. Anapayan et al. [13] presents the details of how these simply supported boundary conditions and loading conditions at the shear centre of LSBs were achieved in the lateral buckling tests of LSBs (Figure 7). The same loading and support boundary conditions were carefully simulated in the finite element model. Single point constraints (SPC) and concentrated nodal forces were used in this model to simulate the experimental boundary conditions and applied loads as closely as possible. The presence of symmetry permitted modelling of only half the span. A 75 mm width clamping plate was connected to the web of the LSB specimen at each support by using four bolts to prevent distortion and twisting of the section (Figure 7(b)). These support plates were simulated using thick shell elements and web mechanical properties. Simply supported boundary conditions were applied to the node at the shear centre in order to provide an ideal pinned support, which was connected to the support plates using four rigid beam MPCs to simulate the bolted connections as used in the experiments (Figure 8(a)).

In the experimental test set-up, a concentrated load was applied at the shear centre at the quarter point of the span using a steel plate (Figure 7(c)). The steel plate was connected to the beam web by using three bolts along the beam centreline. Same loading arrangement was implemented in the experimental finite element model using a concentrated nodal load applied at the cross-section shear centre while simulating the bolts using rigid beam MPCs as shown in Figure 8(b). Thicker shell elements (10 mm) with the mechanical properties of web elements were used to represent the loading plate.

In the preliminary analysis of experimental finite element model the loading plate twisted significantly and influenced the LSB failure direction. This effect was eliminated by providing a twist restraint of SPC "4" (rotation about the longitudinal axis) at the loading point (shear centre) as shown in Figure 8(b).

In the experimental study [13], steel stiffener plates of 6 mm thickness were welded to the inner surfaces of the flanges at each support to prevent localised flange twist except the first four tests. These plates were modelled in the experimental finite element model using the elastic perfect plastic material model and a yield stress of 300 MPa. Figure 9 identifies the various plate elements used with different mechanical properties as defined in ABAQUS. Measured dimensions and yield stresses provided in [13] and Table 4 were used for both the web and flange elements of LSBs.

2.4 Initial Geometric Imperfections

Based on the measurements of initial geometric imperfections and the fabrication tolerance limit for LSBs [13], a value of L/1000 was considered conservatively as the overall geometric imperfection in both the ideal and experimental finite element models of LSBs. A value of depth or width/150 is usually considered as the local plate imperfection. However, local plate imperfection was not considered in the analyses as local buckling mode was not found to be controlling the behaviour of LSBs considered here. The critical imperfection shape was introduced by ABAQUS "*IMPERFECTION" option with the lateral distortional buckling eigenvector obtained from an elastic buckling analysis, and therefore included lateral displacement, twist rotation, and cross section distortion.

Preliminary analyses confirmed the occurrence of lateral distortional buckling for intermediate spans (Figure 2) and revealed that the imperfection direction ("positive" or "negative") influenced the ultimate moment capacity of LSBs subject to lateral buckling. Figures 10 (a) and (b) show the non-linear analysis results of LSBs with positive and negative imperfection shapes. For the beams subject to lateral buckling, negative imperfection was found to be critical and was used in all the non-linear static analyses of ideal LSBs. However, positive imperfection was considered in the experimental finite element models as all the observed experimental failure modes were similar to those with positive imperfections (Figure 17).

2.5 Residual Stresses

The residual stress is an important parameter in the flexural strength of steel beams as this can cause premature yielding, and reduce their flexural strength. Experimental studies showed the presence of both flexural and membrane residual stresses in LSBs due to the use of a combined electric resistance welding and cold-forming process. Figure 11 shows the residual stress distributions of LSBs, which include the flexural residual stress distribution used for all the LSB sections and the membrane residual stress distribution for 200x45x1.6 LSB. Table 2 presents the values of membrane residual stresses for the available 13 LSB sections.

Flexural and membrane residual stresses based on Figure 11 and Table 2 were used in both ideal and experimental finite element models. They were modelled using the ABAQUS *INITIAL CONDITIONS option, with TYPE = STRESS, USER. The user defined initial stresses were created using the SIGINI Fortran user subroutine. This subroutine defines the local components of the initial stress as a function of the global coordinates. The flexural residual stress is also a function of the integration point number through the thickness. As the global coordinates were used to define the local stress components, it was necessary to allow for member imperfections in the calculations. Equations with the member length as a variable and constant deformation factors obtained from the buckling analysis were used to represent the imperfections of top and bottom flanges approximately.

In both the ideal and experimental finite element models of LSBs, the initial stresses were applied in a *STATIC step with no loading and the standard model boundary conditions to allow equilibration of the initial stress field before starting the response history. However, the

equilibration of the initial stress may require additional deformation to bring the model into equilibrium due to the unbalanced stress. Past research on hot-rolled I-sections [19] considered an additional "force field" in the *STATIC step to reverse this additional initial deformation. This technique was not considered since it introduced additional restraint to the section in the subsequent non-linear analysis step, and the initial deformation effect was considered to be insignificant.

2.6 Analysis Methods

Two methods of analysis, elastic buckling and nonlinear static analyses, were used in this study. Elastic buckling analyses were carried out first and were used to obtain the eigenvectors for the inclusion of geometric imperfections. Nonlinear static analysis, including the effects of large deformation and material yielding, was adopted to investigate the behaviour of LSB sections up to failure. ABAQUS uses the Newton-Raphson method to solve the non-linear equilibrium equations. The RIKS method in ABAQUS was also included in the nonlinear analysis. It is generally used to predict geometrically unstable nonlinear collapse of structures. The RIKS method uses the load magnitude as an additional unknown and solves simultaneously for loads and displacements. Therefore, another quantity should be used to measure the progress of the solution. For this purpose, ABAQUS uses variable arc-length constraint to trace the instability problems associated with nonlinear buckling of beams. The parameters used for non-linear static analyses are as follows:

- Typical maximum number of load increments = 100,
- Initial increment size = 0.0001,
- Minimum increment size = 0.0000001,
- Automatic increment reduction enabled, and large displacements enabled.

The finite element models of LSBs were developed in MD R2.1/PATRAN and submitted to ABAQUS (Version 6.7-1) for analysis.

3. Validation of Finite Element Models

The accuracy of the developed finite element models was verified by conducting two series of comparisons. In the first series the elastic lateral distortional buckling moments obtained using the ideal finite element model were compared with the corresponding elastic buckling moments from the established finite strip analysis program, Thin-Wall, and Pi and Trahair's [12] equations (Section 3.2). In the second series, the experimental results of LSBs subject to

lateral distortional buckling as reported in [13] were compared with the results from the non-linear static analyses of the experimental finite element model (Section 3.3).

3.1 Typical Buckling Modes of Ideal Finite Element Model

Elastic buckling analysis results showed that LSBs exhibited three distinct buckling modes, namely, local buckling for short spans, lateral distortional buckling for intermediate spans and lateral torsional buckling for long spans. They confirmed that the LSBs with intermediate spans in the range of 1500 mm to 6000 mm are prone to lateral distortional buckling (smaller sections exhibited lateral distortional buckling at 750 mm and lateral torsional buckling from about 5000 mm). The level of web distortion in lateral distortional buckling reduced with increasing beam slenderness, and thus approached lateral torsional buckling. These observations agree well with those in the experimental study [13].

Figures 12 (a) to (d) show these three buckling modes of 200x60x2.0LSB from the elastic buckling analyses while Figures 13 (a) and (b) show their ultimate failure modes of 200x60x2.0 LSB from the nonlinear static analyses based on the ideal finite element model. For LSBs with 500 mm span, yielding occurred before local buckling at ultimate failure (Figure 15(a)) and the ultimate capacity is their section moment capacity. When a positive imperfection was included, the lateral distortional and lateral torsional buckling failure modes were similar to those exhibited in elastic buckling analyses (Figures 12 (b) and (c)) while a failure mode shown in Figure 13 (b) was observed for LSBs with a negative imperfection.

3.2 Comparison of Elastic Buckling Moment Results

Elastic buckling moment results from the ideal finite element model were compared with the corresponding solutions obtained from Thin-Wall, and Pi and Trahair's [12] equations for elastic lateral distortional buckling moment, M_{od}, given next.

$$M_{od} = \sqrt{\frac{\pi^2 EI_y}{L^2}\left(GJ_e + \frac{\pi^2 EI_w}{L^2}\right)} \qquad (1)$$

where

EI_y = minor axis flexural rigidity

EI_w = warping rigidity

GJ_e = effective torsional rigidity as given by Eq.2

L = span

$$GJ_e = \frac{2GJ_f\left(\frac{Et^3L^2}{0.91\pi^2 d_1}\right)}{2GJ_f + \left(\frac{Et^3L^2}{0.91\pi^2 d_1}\right)} \quad (2)$$

where

GJ_f = flange torsional rigidity

t = nominal thickness

d_1 = clear depth of the web

Elastic buckling moments from FEA, Thin-Wall and Pi and Trahair's [12] equations and the differences are given in Table 3 for two LSBs while others are given in [14]. The comparison of elastic buckling moments from the three methods is also shown in Figure 14 as a plot of elastic buckling moment versus span for other LSBs. The comparison shows that FEA results agree well with the results from both Thin-Wall and Pi and Trahair's [12] equations, where the average difference is about 1.5% and 2.9%, respectively. Considering the fact that Pi and Trahair's [12] equations give an approximate solution, the observed difference of 2.9% is acceptable. The smaller difference of 1.5% with Thin-Wall may be due to a very fine mesh density used in the finite element model. Most of the larger LSB sections exhibited local buckling at 1000 mm span as shown in Table 3. Local buckling moments from FEA agreed very well with Thin-Wall results with a percentage difference of less than 1% on average. Pi and Trahair's [12] equations only provide solutions for M_{od}, and thus its results for short spans cannot be compared with FEA results.

Based on Table 3 and Figure 14, it can be confirmed that the ideal finite element model developed in this research accurately predicts the elastic lateral distortional buckling moments of LSBs. These comparisons verify the suitability and accuracy of the element type, mesh density, geometry, boundary conditions and the method used to apply a uniform bending moment.

3.3 Comparison of Ultimate Moment Capacities with Experimental Test Results

For this purpose 11 test results from Test Series 2 in [13], representing different LSBs and spans were used. The first four tests did not use the stiffener plates to provide local flange

twist restraints at the supports and hence the corresponding experimental finite element models also did not include them. Table 4 compares the ultimate moment capacity results from experiments and the non-linear static analyses using the experimental finite element model. A comparison of FEA and experimental test results is also provided in the form of typical bending moment versus vertical deflection curves in Figures 15 (a) and (b) for some LSBs. The vertical deflection was taken at the centre of the web at mid-span. A good agreement can be seen between the experimental and FEA results. Typical bending moment versus lateral deflection curves are also provided in Figures 16 (a) and (b). These figures compare the measured experimental lateral deflections at mid-span for both the top and bottom flanges with corresponding deflections predicted by FEA. The agreement in this case is also considered reasonably good. Comparison of load-deflection curves for other LSBs are given in [14].

Figure 17 (a) shows the predicted failure mode of 200x45x1.6 LSB based on the experimental finite element model with positive imperfections. This compares well with the observed lateral distortional buckling failure in the experimental study as shown in Figure 17 (b).

The comparisons provided in Table 4 and Figures 15 to 17 demonstrate that the experimental finite element model predicts the ultimate failure moments, failure modes and the moment-deflection characteristics accurately. The mean ratio of the ultimate moment capacity from the finite element model and experiment was 0.99 with a COV of 0.047. This result suggests that the developed finite element model is accurate, considering the possible sources of error due to unavoidable differences between the experimental test and finite element model.

Anapayan et al. [13] presents the details of Test Series 1 that were not considered here. Mahaarachchi and Mahendran [20] presents the comparison of the ultimate moment capacities from these tests and a finite element model similar to the experimental finite element model used here. They also found a good agreement between FEA and experimental results.

In summary, the developed finite element model provided close comparisons with experimental results. It is therefore reasonable to assume that these comparisons establish the validity of the shell element model for explicit modelling of initial geometric imperfections and residual stresses, lateral distortional and local buckling deformations, and associated material yielding effects in LSB flexural members. The suitability of the residual stress

model, geometric imperfection magnitudes, and the finite element mesh density has also been verified.

4. Parametric Study

In the parametric study the validated ideal finite element model of LSBs with simply supported conditions and a uniform moment as described in Section 2 was used to analyse the lateral buckling behaviour of 13 LSBs with spans varying from 1 to 10 m and develop an extensive data base of member moment capacities. In order to save time in model preparation, PATRAN database journal file containing instructions for the pre-processor was used to automatically generate a model for varying spans. The created ABAQUS input files were analysed using the bifurcation buckling solution sequence to obtain the elastic buckling eigenvectors. The global geometric imperfections and residual stresses were then included in the nonlinear analysis model, and the analysis was continued using the nonlinear static solution sequence.

Based on AS/NZS 4600 [21] design rules for local buckling, the web and flange plate elements of all the LSB sections are fully effective if corners are included. However, if corners are not included as assumed in FEA, the effective section moduli of five LSB sections are about 2% less than their full section moduli. Local buckling could therefore occur in these slender LSB sections with short spans. However, the ultimate moment capacity results of such cases were not considered in this research as it was focussed on lateral buckling. An associated research report provides the section moment capacity results of LSBs subject to local buckling [22].

Figure 18 presents the ultimate moment capacity results of LSBs subject to lateral distortional and lateral torsional buckling as a function of span. For LSBs with intermediate slenderness, the moment capacity is reduced below the first yield moment due to the interaction of yielding and buckling effects. This inelastic lateral distortional buckling capacity is influenced by residual stresses and initial geometric imperfections. For LSBs with high slenderness, the ultimate moment capacity can be predicted approximately by the elastic lateral distortional buckling moment M_{od}. This indicates that the effects of yielding, residual stresses and initial geometric imperfections are very small for slender beams.

In the parametric study, the effects of initial geometric imperfection and residual stresses were further investigated. Both positive and negative initial geometric imperfections of magnitude L/1000 were included in FEA of five LSBs without residual stresses, and the results showed that the ratio of ultimate moments of LSBs with negative and positive imperfections varied from 0.87 to 0.95 with the higher ratios for larger spans. These results confirm that the use of negative imperfection is critical as the ultimate moments were lower for LSBs with negative imperfections than for positive imperfections. When the effects of residual stresses were investigated using nonlinear analyses of five LSBs with the critical negative initial imperfection, it was found that the use of residual stresses significantly reduced the moment capacities of LSBs in the case of intermediate spans while their effect is not significant for large spans. The ratios of ultimate moment capacities of LSBs with and without residual stresses varied from 0.82 to 0.94. The results also showed that the effect of residual stress is significant for slender LSBs in comparison with compact LSBs. Further results of the effects of initial imperfections and residual stresses on the member moment capacities of LSBs are given in [23].

5. Comparison of Member Moment Capacities with AS/NZS 4600 [21] Design Rules

In this section, the ultimate moment capacities of LSBs from FEA are compared with the predictions from the current design rules in AS/NZS 4600 [21] for members subject to lateral distortional buckling. The member moment capacity, M_b, is given by Equation 1:

$$M_b = M_c\left(\frac{Z_e}{Z}\right) \qquad (3)$$

where

Z = full section modulus

M_c = critical moment

Z_e = effective section modulus

For LSBs, it is appropriate to determine the effective section modulus at a stress corresponding to M_c/Z, where M_c is defined in Equation 4.

For $\lambda_d \leq 0.59$: $M_c = M_y$ (4a)

For $0.59 < \lambda_d < 1.70$: $M_c = M_y\left(\frac{0.59}{\lambda_d}\right)$ (4b)

For $\lambda_d \geq 1.70$: $$M_c = M_y\left(\frac{1}{\lambda_d{}^2}\right) \quad (4c)$$

where

λ_d = member slenderness (Equation 5)

M_y = first yield moment

$$\lambda_d = \sqrt{\frac{M_y}{M_{od}}} \quad (5)$$

The elastic lateral distortional buckling moment M_{od} can be calculated using Pi and Trahair's [12] equations as provided in Equations 1 and 2 or an elastic buckling analysis program such as Thin-Wall or CUFSM.

Figure 19 compares the member moment capacities from FEA with the AS/NZS 4600 [21] design curve based on the above equations. The ultimate moment capacities (M_u) and the elastic lateral distortional buckling moments (M_{od}) were obtained from FEA while the first yield moments (M_y) were obtained by using Equation 6.

$$M_y = Z\, f_y \quad (6)$$

The corners of LSBs were ignored in the calculation of section properties (Z) since the finite element models also did not include the corners (Table 1). The nominal flange yield stress of 450 MPa was used to calculate M_y. The values of M_u, M_{od} , M_y, M_u/M_y and λ_d of some LSBs with varying spans used in the comparison in Figure 19 are given in Table 5, while these values for other LSBs and spans are provided in [23].

The effective section moduli (Z_e) of LSB sections calculated based on AS/NZS 4600 [21] show that some LSB sections without corners are likely to exhibit local buckling effects as their Z_e values are about 2% less than their Z values when the maximum compressive stress is taken as its yield stress (450 MPa) [23]. However, only the FEA moment capacities of LSB members subject to lateral distortional and lateral torsional buckling are considered in this research in the comparison with design rules. Therefore there is no need to allow for any local buckling effects as a result of the reduced Z values of some LSB sections.

Figure 19 clearly shows that almost all the FEA data points are above the current design curve for intermediate slenderness (inelastic lateral buckling region). Experimental study [13] also showed that the moment capacities of LSBs were higher than the predictions from the current design rule in the inelastic region. The member moment capacities from FEA and AS/NZS 4600 [21] were compared for each LSB and span in [23] (Table 5). The mean and COV values of the ratio of member moment capacities from FEA and AS/NZS 4600 are 1.08 and 0.088 for LSBs within the inelastic lateral buckling region ($0.59 < \lambda_d < 1.70$). For these calculated mean and COV values, a capacity reduction factor (Φ) of 0.96 was determined using the recommended AISI procedure, which is based on a statistical model allowing for the variations in material, fabrication and loading effects [24] and a target reliability index of 2.5. This Φ value is greater than the recommended factor of 0.90 in AS/NZS 4600 [21] for flexural members and hence confirms that the current AS/NZS 4600 design rule is conservative in the inelastic lateral buckling region.

6. Proposed Design Rules for Member Moment Capacities of LSBs

When the member moment capacity results from FEA in this study and experiments [13] were compared with the predictions from the current design rules in AS/NZS 4600 [21] it was found that the current design rule is conservative in the inelastic buckling region while it is adequate in the elastic buckling region. Therefore the member moment capacity results from experiments and FEA were combined and used to improve the current design equations. Experiments and FEA reveal the presence of at least three buckling modes for LSB flexural members, namely, local, lateral distortional and lateral torsional buckling. Current design rules consider three distinct regions such as local buckling/yielding, inelastic and elastic buckling regions, which correspond to the above buckling modes. Since the current design rule accurately predicts the moment capacities of LSBs in the elastic buckling region (mostly subject to lateral torsional buckling), a new design rule was developed for the inelastic lateral distortional buckling region. The new design equation was established by solving for minimum total error for all the 13 LSB sections and spans considered here. This was achieved by minimising the square of the difference between the non-dimensionalised moment capacity results (M_u/M_y) from FEA and experiments and that predicted by the new equation (M_b/M_y). The new design rule for the inelastic buckling region is given by Equation 7(b) and Figure 20 compares the design curve based on this equation with the current AS/NZS 4600 design curve and FEA and experimental results.

For $\lambda_d \leq 0.54$: $M_c = M_y$ (7a)

For $0.54 < \lambda_d < 1.74$: $M_c = M_y (0.28 \lambda_d^2 - 1.20 \lambda_d + 1.57)$ (7b)

For $\lambda_d \geq 1.74$: $M_c = M_y \left(\frac{1}{\lambda_d^2} \right)$ (7c)

The use of FEA provided a large number of moment capacity results (about 110 results in this research) [23]. However, experimental results are also needed to demonstrate the accuracy of developed design rules. In this research the developed design rules were calibrated using FEA and experimental moment capacity results separately and in combination as shown in Table 6. The mean and COV values of the ratios of ultimate member moment capacities from FEA, experiments and FEA and experiments, and Eq.7 (b) were calculated, ie. FEA / Eq.7 (b), Test / Eq.7 (b) and (FEA + Test) / Eq.7 (b), and are presented in Table 6. The corresponding capacity reduction factors (Φ) were also determined using the AISI procedure [24].

As seen in Table 6, a capacity reduction factor of 0.92 was obtained for FEA results, which is greater than the recommended factor of 0.90 in AS/NZS 4600 [21]. However, it was 0.86 for experiments, which is less than the recommended value. This is because of comparatively low mean and high COV values of the ratios of experimental to predicted moment capacities. As shown in Figure 20, most of the experimental data points of Test Series 1 in [13] were below the developed design curves which caused the reduction of the mean value. This may be due to the approximate M_{od} values used in plotting the data points. The M_{od} value was calculated using Thin-Wall for Test Series 1 [13]. Thin-Wall assumes ideal simply supported conditions although localised flange twist was not fully eliminated in these tests. The use of accurate M_{od} values for these tests would have given higher ratios of test/predicted moment capacities and hence a greater capacity reduction factor as discussed in [13]. Nevertheless, the capacity reduction factor was 0.90 when both FEA and experimental results were considered, and this is considered adequate. Therefore it is recommended that the developed design equation (Eq.7 (b)) can be used in the design of LSBs with a capacity reduction factor of 0.90 within the guidelines of AS/NZS 4600 [21].

7. Conclusions

This paper has described the details of two finite element models developed for the investigation into the behaviour of LSB flexural members subject to lateral buckling and a detailed parametric study based on validated models. The first model referred to as the ideal model was developed to simulate the behaviour of LSBs with idealised simply supported conditions subject to a uniform bending moment whereas the second model referred to as the experimental model was developed to simulate the LSB flexural members subject to quarter point loading as used in the experimental study reported in [13]. The models were validated by the comparison of elastic buckling and ultimate moment capacity results with corresponding results from an established finite strip analysis program (Thin-Wall) and Pi and Trahair's [12] equations, and experimental test results, respectively. They accurately predicted both the elastic lateral distortional buckling moments and the non-linear ultimate moment capacities of LSBs. The models accounted for all the significant behavioural effects including material inelasticity, lateral distortional buckling deformations, web distortion, residual stresses, and geometric imperfections. The use of validated ideal finite element model in a detailed parametric study produced valuable moment capacity data for LSBs and most importantly, improved design rules for LSB flexural members subject to lateral distortional buckling.

Acknowledgements

The authors would like to thank Australian Research Council and OATM for their financial support and the Queensland University of Technology for providing the necessary facilities and support to conduct this research project. They would also like to thank Mr Ross Dempsey, Manager - Research and Testing, OATM for his technical contributions, and his overall support to the many different phases of this research project.

References

[1] OneSteel Australian Tube Mills, (OATM), LiteSteel Beam Publication, Brisbane, Australia, 2008.

[2] Timoshenko, S.P. and Gere, G.M., Theory of Elastic Stability, 2nd Edition, McGraw-Hill Book Co. Inc., New York, USA, 1961.

[3] Trahair, N.S., Flexural Torsional Buckling of Structures, E and FN Spon, London, UK, 1993.

[4] Yu, W.W., Cold-Formed Steel Design, 3rd edition, John Wiley & Sons Inc. New York, USA, 2000

[5] Hancock, G. J., Bradford, M.A. and Trahair, N.S., Web Distortional and Flexural-Torsional Buckling, ASCE Journal of the Structural Division, Vol.106 (7), pp.1557-1571, 1980.

[6] Bradford, M.A., Lateral Distortional Buckling of Steel I-Section Members", Journal of Construction Steel Research, Vol.23, pp.97-116, 1992.

[7] Dempsey, R.I., Structural Behaviour and Design of Hollow Flange Beams, Proceedings of the 2nd National Structural Engineering Conference, Institution of Engineers, Barton, ACT, Australia, pp.325-335, 1990.

[8] Mahendran, M. and Doan, V., Lateral Distortional Buckling Tests of Hollow Flange Beams, Research Monograph 99-3, Queensland University of Technology, Brisbane, Australia, 1999.

[9] Avery, P., Mahendran, M. and Nasir, A., Flexural Capacity of Hollow Flange Beams, Journal of Construction Steel Research, Vol.53, pp.201-223, 2000.

[10] Avery, P. and Mahendran, M., Finite Element Analysis of Hollow Flange Beams with Web Stiffeners", ASCE Journal of Structural Engineering, Vol.123, No.9, pp.1123-1129, 1997.

[11] Mahendran, M. and Avery, P., Bucking Experiments on Hollow Flange Beams with Web Stiffeners, ASCE Journal of Structural Engineering, Vol.123, No.9, pp.1130-1134, 1997.

[12] Pi, Y.-L. and Trahair, N. S., Lateral Distortional Buckling of Hollow Flange Beams, ASCE Journal of Structural Engineering, Vol.123, No.6, pp.695-702, 1997.

[13] Anapayan, T., Mahendran, M. and Mahaarachchi, D. Lateral Distortional Buckling Tests of a New Hollow Flange Channel Beam, Thin-Walled Structures, Vol.49, Issue 1, pp. 13-25, 2011.

[14] Anapayan, T. and Mahendran, M., Finite Element Models of LiteSteel Beams Subject to Lateral Buckling Effects, Research Report, Queensland University of Technology, Brisbane, Australia, 2009.

[15] Hibbit Karisson and Sorensen, ABAQUS User's Manual, Pawtucket, RI., USA, 2007.

[16] Ashraf, M., Gardner, L. and Nethercot, D. A., Finite Element Modelling of Structural Stainless Steel Cross-Sections, Thin-Walled Structures, Vol.44, pp.1048-1062, 2006.

[17] Kurniawan, C.W. and Mahendran, M., Elastic Lateral Buckling of Simply Supported LiteSteel Beams Subject to Transverse Loading, Thin-Walled Structures, Vol.47, pp.109-119, 2009.

[18] Zhao, X. L., Hancock, G. J. and Trahair, N. S., Lateral Buckling Tests of Cold-Formed RHS Beams, ASCE Journal of Structural Engineering, Vol.121, No.11, pp.1565-1573, 1995.

[19] Yuan, Z., Advanced Analysis of Steel Frame Structures Subjected to Lateral Torsional Buckling Effects, PhD Thesis, Queensland University of Technology, Brisbane, Australia, 2004.

[20] Mahaarachchi, D. and Mahendran, M., Finite Element Analysis of LiteSteel Beam Sections, Research Report No.3, Queensland University of Technology, Brisbane, Australia, 2005.

[21] Standards Australia/Standards New Zealand, AS/NZS 4600 Cold-Formed Steel Structures, Sydney, Australia, 2005.

[22] Anapayan, T., Mahendran, M. and Mahaarachchi, D. Section Moment Capacities of LiteSteel Beams, Thin-Walled Structures, Vol.49, Issue 4, pp.502-512, 2011.

[23] Anapayan, T. and Mahendran, M., Parametric Studies and Development of Design Rules for LiteSteel Beams Subject to Lateral Buckling, Research Report, Queensland University of Technology, Brisbane, Australia, 2009

[24] American Iron and Steel Institute (AISI) (2007), North American Specification for the Design of Cold-formed Steel Structural Members, AISI, Washington, DC, USA, 2007.

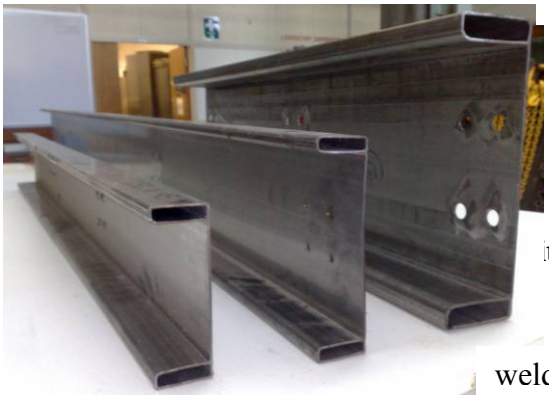

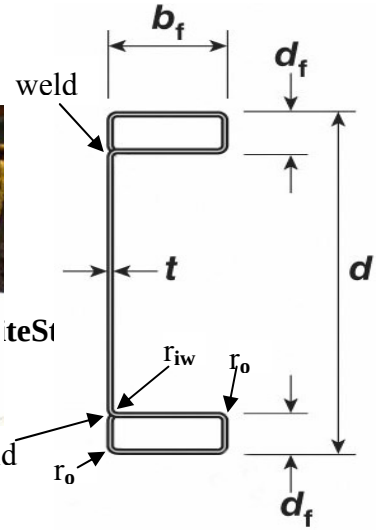
b_f
d_f
weld
t
d
r_{iw}
r_o
weld
r_o
d_f

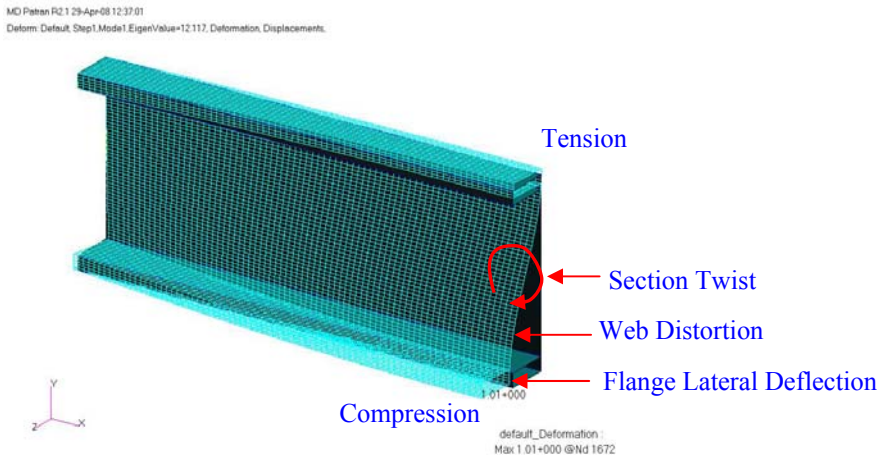

Figure 2: Lateral Distortional Buckling of LSBs

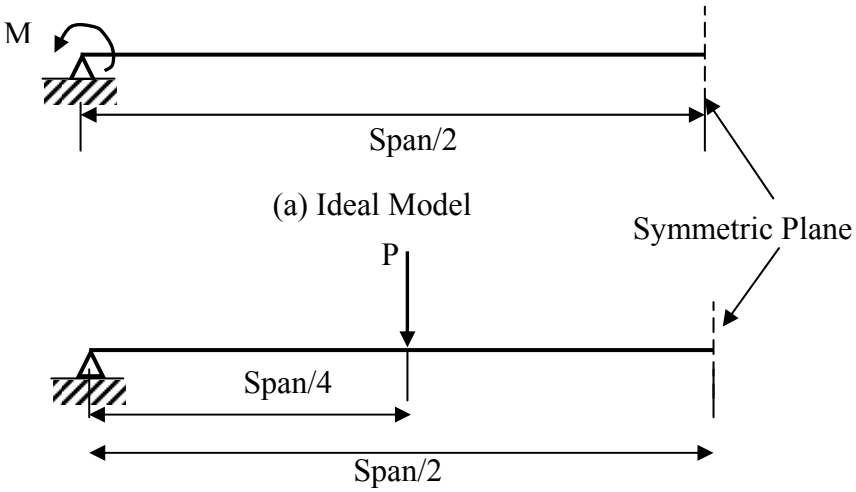

(a) Ideal Model

(b) Experimental Model

Figure 3: Ideal and Experimental Finite Element Models

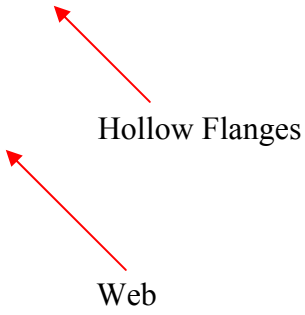

Figure 4: Typical Finite Element Mesh for LSB Models

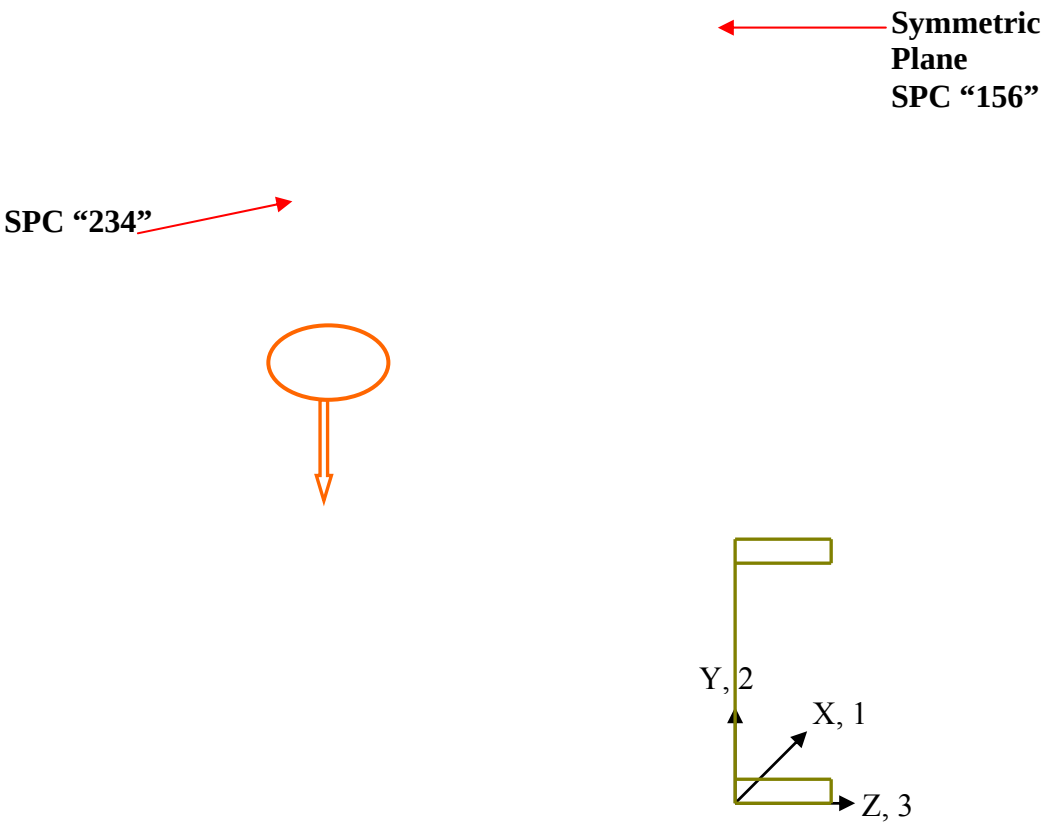

Figure 5: Boundary Conditions of the Ideal Finite Element Model of LSB

Figure 6: Typical Loading Method for the Ideal Finite Element Model of LSB

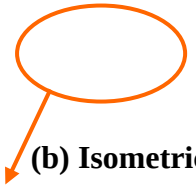

(a) Front View **(b) Isometric View**

(c) Close-up View

(a) Quarter Point Loading of LSB

(a) Overall Test Set-up

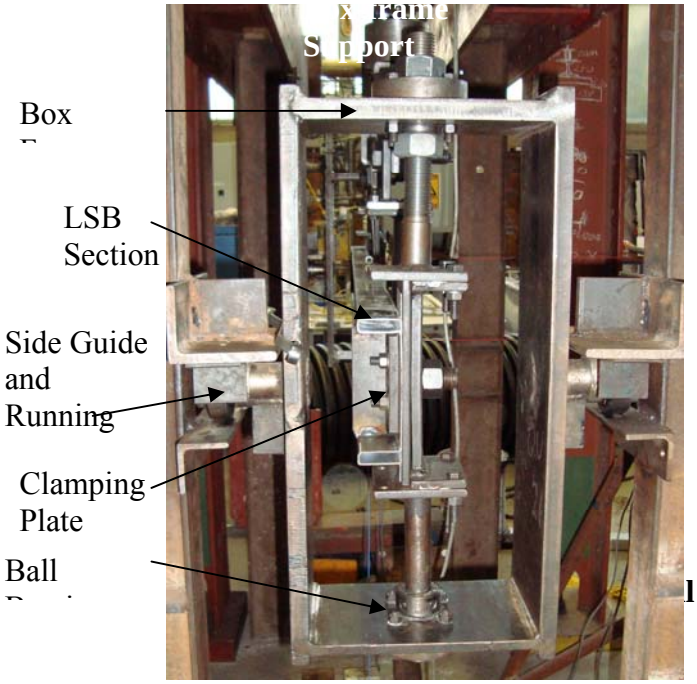

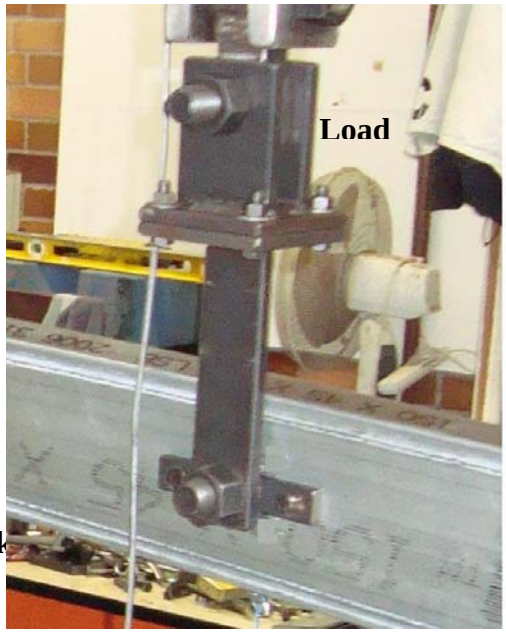

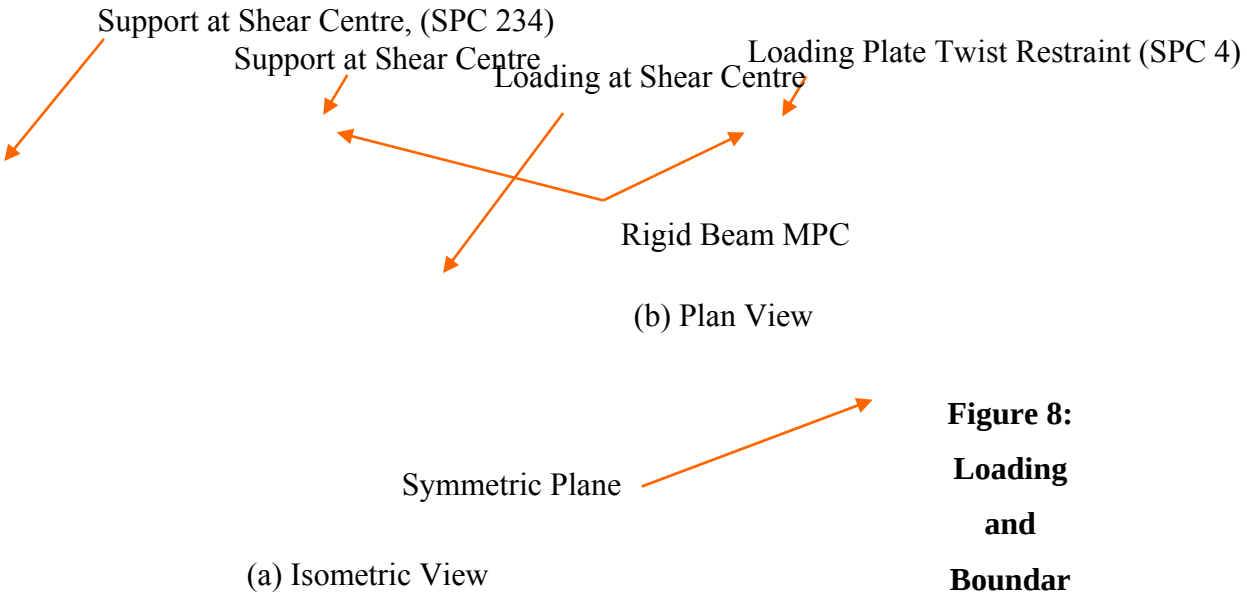

Figure 8: Loading and Boundary Conditions of the Experimental Finite Element Model of LSB

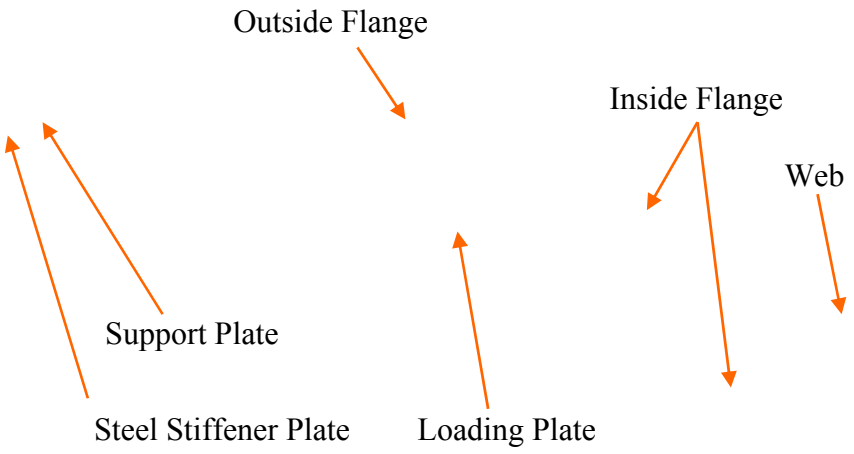

Figure 9: Various Plate Elements Used in Experimental Finite Element Model

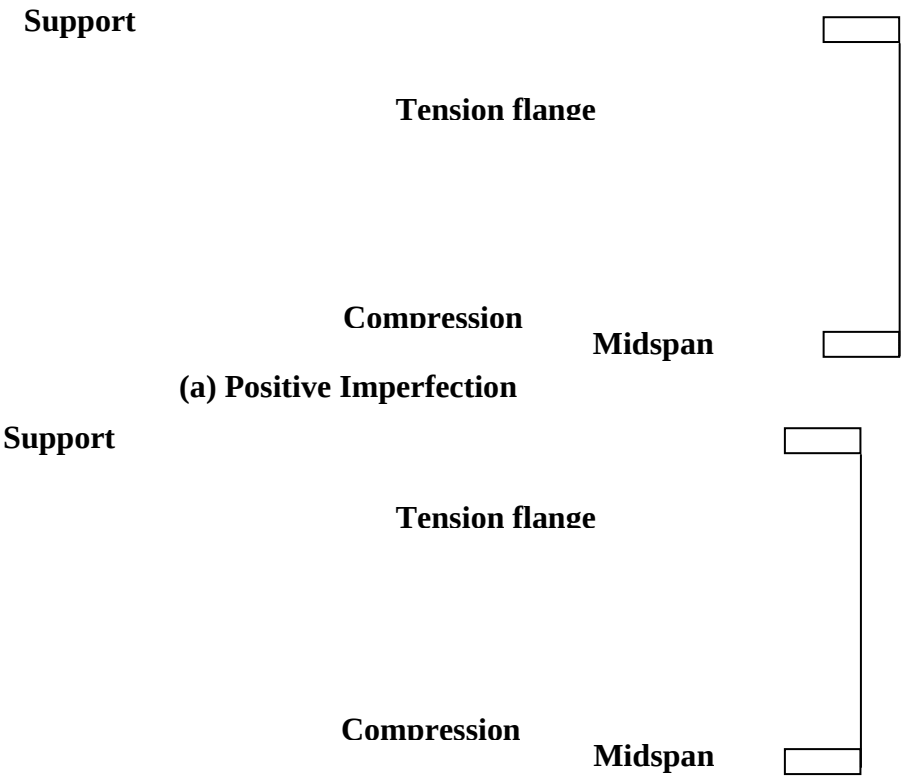

Figure 10: Effect of Imperfection Direction

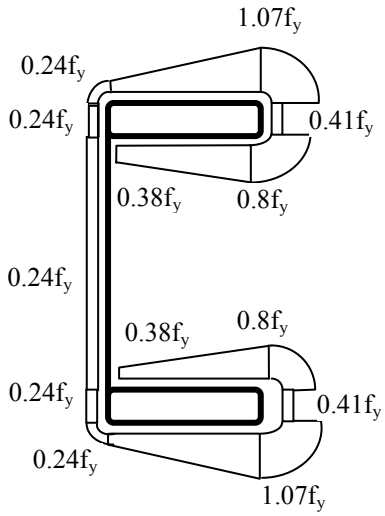

(a) Flexural Residual Stress

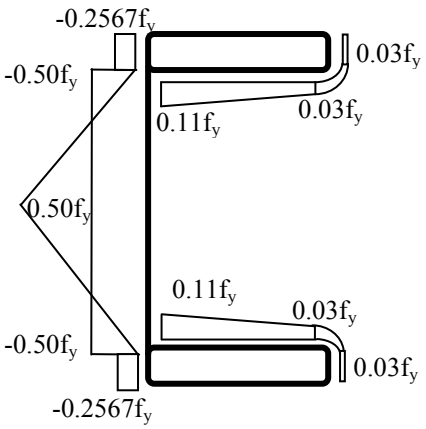

(b) Membrane Residual Stress for 200x45x1.6LSB

Figure 11: Residual Stress Distributions in LSB Sections [13]

(a) Local Buckling (500 mm)

(b) Lateral Distortional Buckling (4000 mm)

(c) Lateral Torsional Buckling (8000 mm)

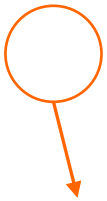

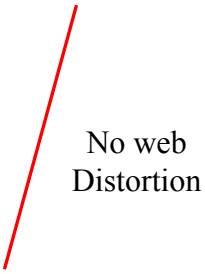

(d) Close-up View (LTB)

Figure 12: Elastic uckling Modes of 200x60x2.0 LSB

(b) LDB

Figure 13: Ultimate Failure Modes of 200x60x2.0 LSB

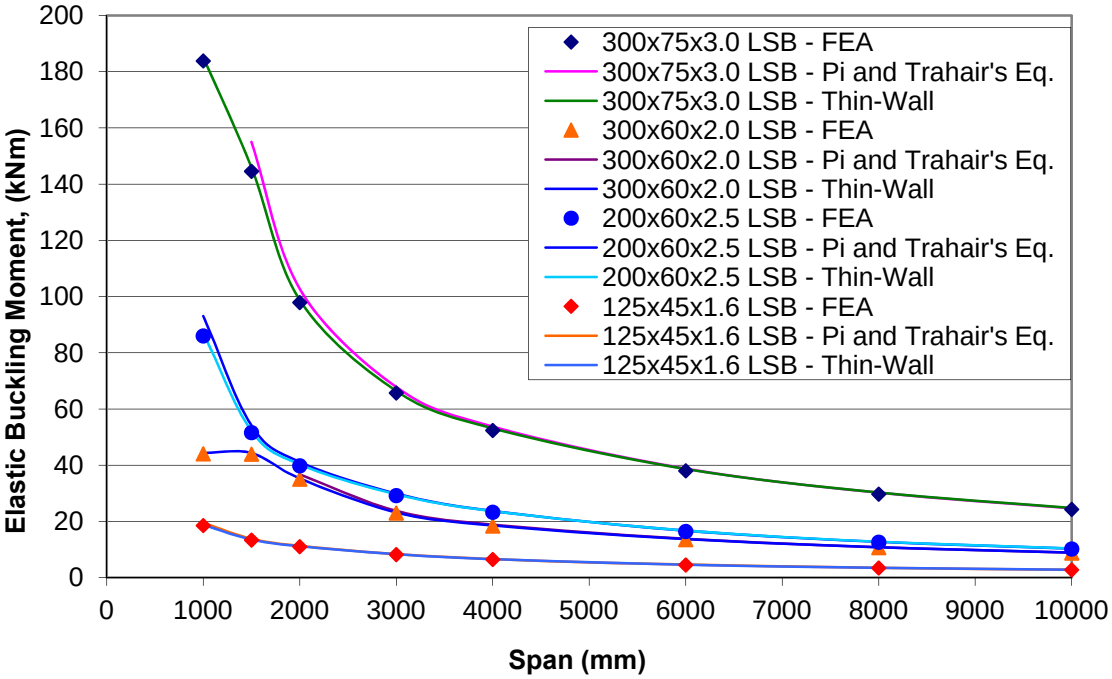

Figure 14: Comparison of Elastic Buckling Moments

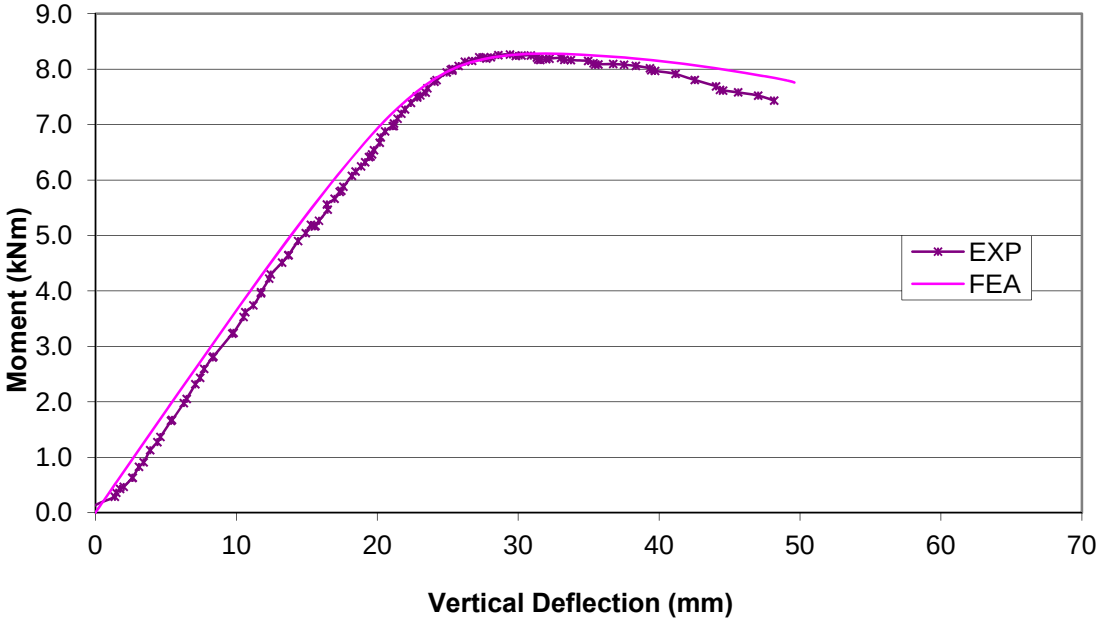

(a) 3000 mm span 150x45x1.6 LSB

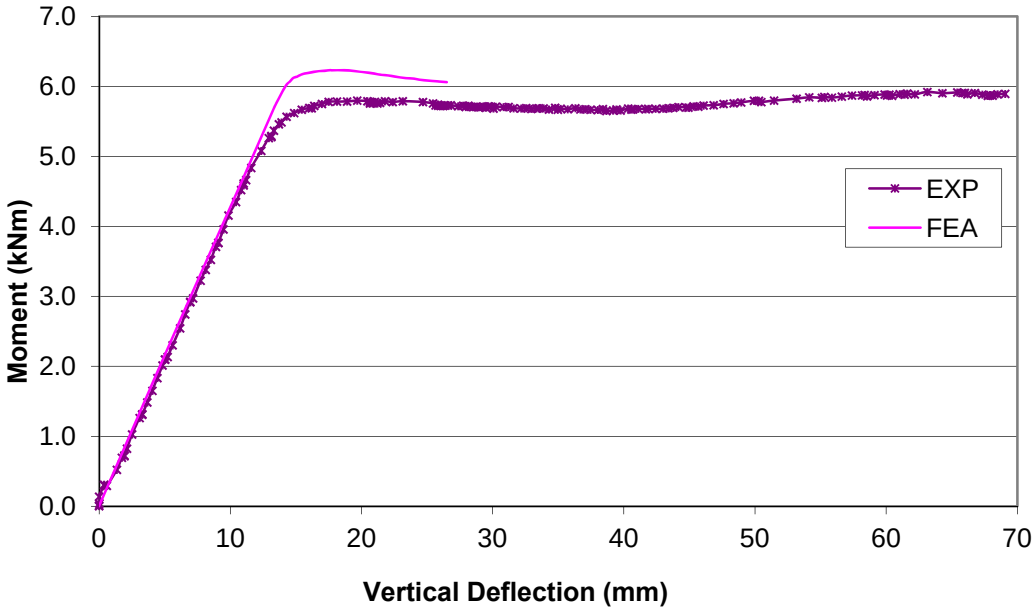

(b) 4000 mm Span 200x45x1.6 LSB

Figure 15: Bending Moment versus Vertical Deflection at Mid-Span Curves

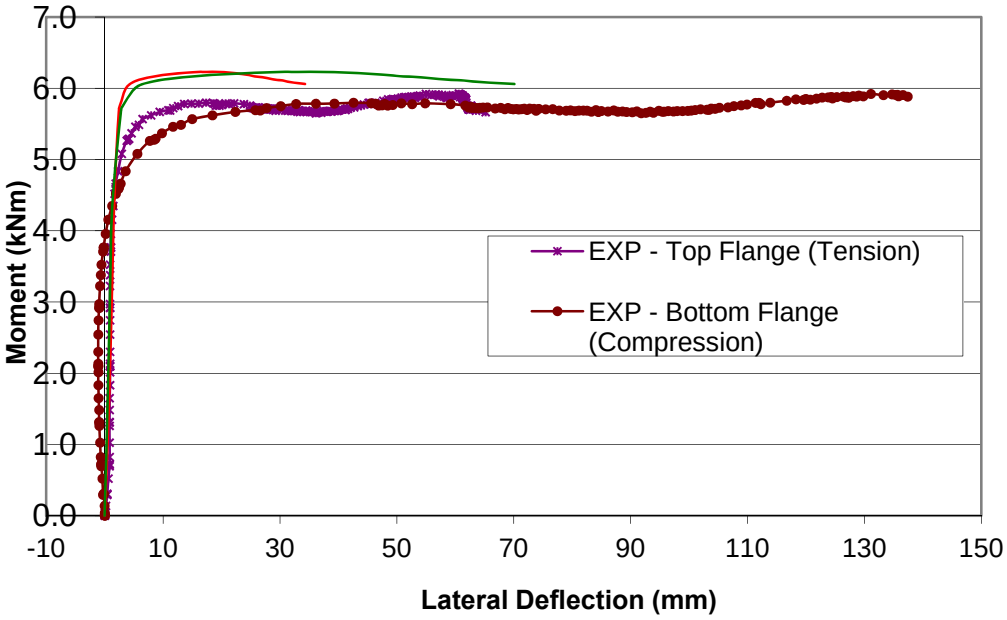

(a) 4000 mm Span 200x45x1.6 LSB

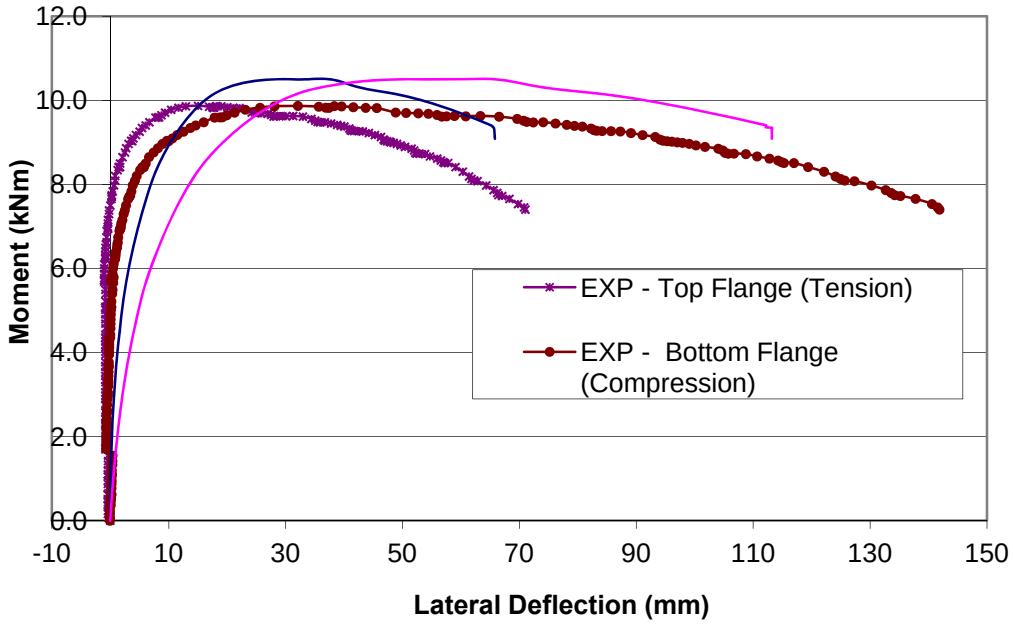

(b) 3000 mm Span 150x45x2.0 LSB

Figure 16: Bending Moment versus Lateral Deflection at Mid-Span Curves

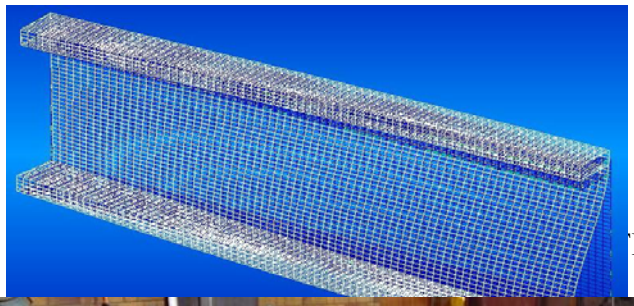

TEA

(b) Experiments [13]

Figure 17: Comparison of Failure Mode of 200x45x1.6 LSB

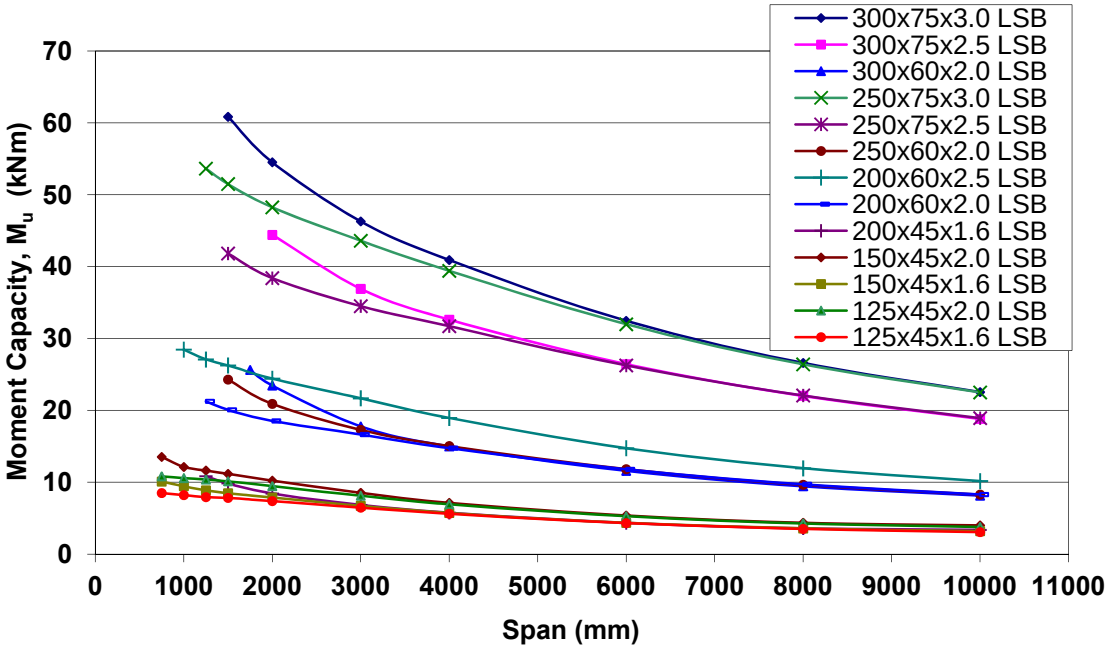

Figure 18: Ultimate Moment Capacity Curves of LSBs

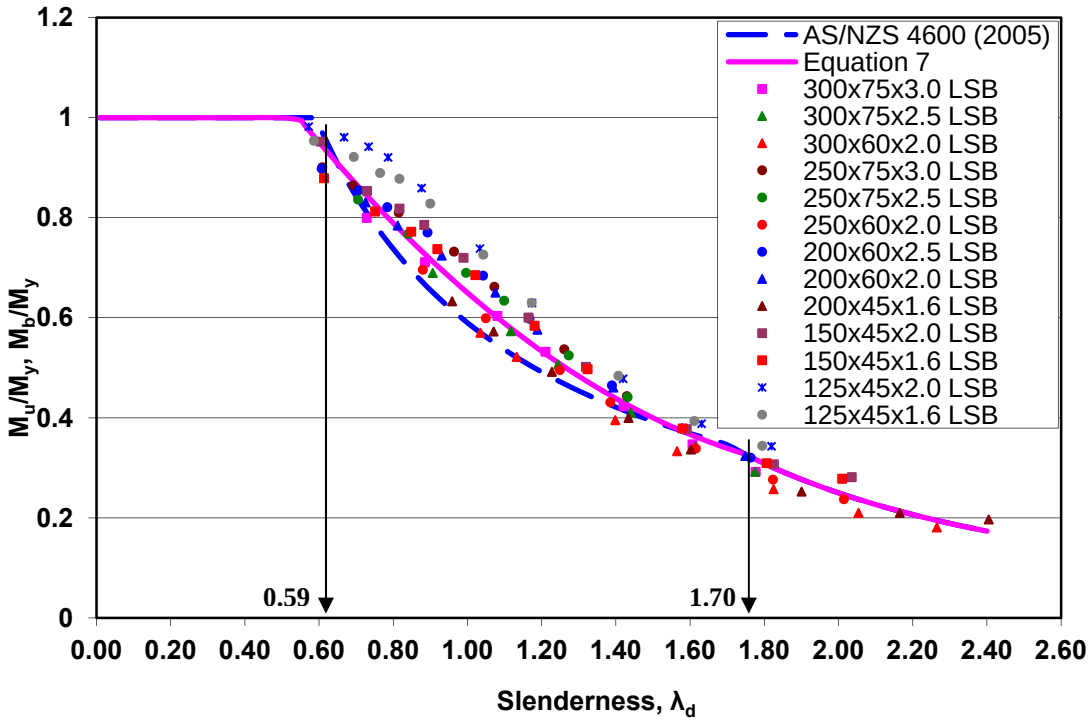

Figure 19: Comparison of Moment Capacity Results from FEA with AS/NZS 4600 Design Curve

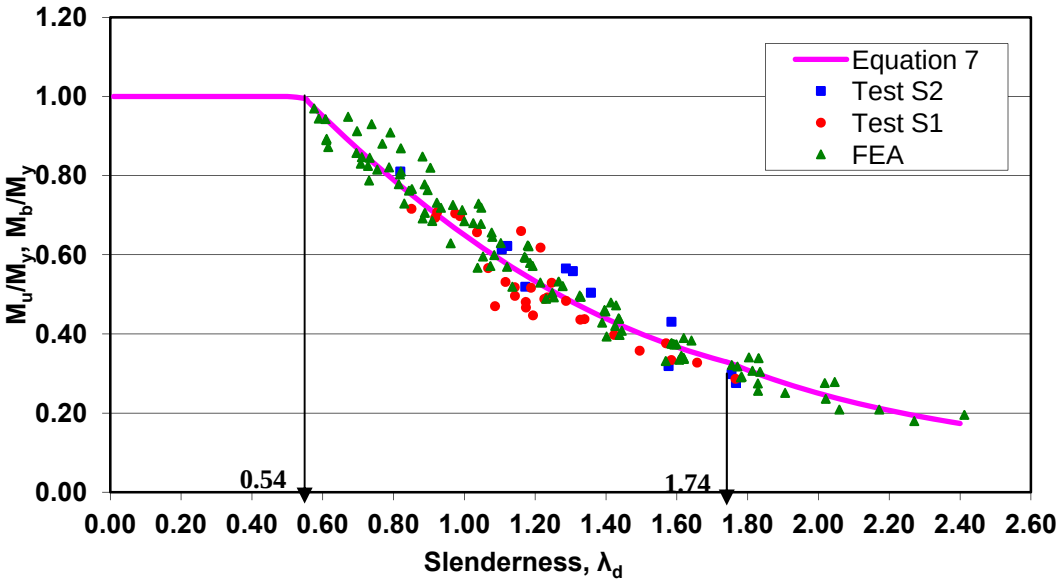

Figure 20: Comparison of FEA and Experimental Moment Capacities with the Design Curve based on Equations 7 (a) to (c)

Table 1: Details of Currently Available LSB Sections

LSB Section	d	d_1	b_f	d_f	t	r_o	r_{iw}	Elastic Section Modulus Z ($x10^3$)	
								RC	RAC
	mm	mm	mm	mm	mm	mm	mm	mm^3	mm^3
300x75x3.0	300	244	75	25	3.0	6.0	3.0	166.8	171.7
300x75x2.5	300	244	75	25	2.5	5.0	3.0	140.6	144.0
300x60x2.0	300	254	60	20	2.0	4.0	3.0	98.2	100.4
250x75x3.0	250	194	75	25	3.0	6.0	3.0	129.5	133.5
250x75x2.5	250	194	75	25	2.5	5.0	3.0	109.2	112.0
250x60x2.0	250	204	60	20	2.0	4.0	3.0	76.2	78.0
200x60x2.5	200	154	60	20	2.5	5.0	3.0	68.9	71.1
200x60x2.0	200	154	60	20	2.0	4.0	3.0	55.9	57.3
200x45x1.6	200	164	45	15	1.6	3.2	3.0	37.4	38.3
150x45x2.0	150	114	45	15	2.0	4.0	3.0	30.8	31.9
150x45x1.6	150	114	45	15	1.6	3.2	3.0	25.1	25.7
125x45x2.0	125	89	45	15	2.0	4.0	3.0	23.9	24.8
125x45x1.6	125	89	45	15	1.6	3.2	3.0	19.5	20.0

Note: d–depth, d_1–clear web depth, b_f – flange width, d_f – flange depth, t – thickness, r_o – outer corner radius, r_{iw} – inner corner radius, RC – Rounded Corners, RAC – Right Angle Corners

Table 2: Membrane Residual Stress Distribution of LSB Sections

LSB	Centreline Dimensions (mm)					Membrane Residual Stress as a Ratio of f_y					
	d	d_1	b_f	d_f	t	Left Flange	Right Flange	Web Top	Mid Web	Inside Flange Left	Inside Flange Right
300x75x3.0	297.0	247.0	72.0	22.0	3.0	-0.2591	0.03	-0.50	0.50	0.11	0.03
300x75x2.5	297.5	247.5	72.5	22.5	2.5	-0.2556	0.03	-0.50	0.50	0.11	0.03
300x60x2.0	298.0	258.0	58.0	18.0	2.0	-0.2556	0.03	-0.50	0.50	0.11	0.03
250x75x3.0	247.0	197.0	72.0	22.0	3.0	-0.2591	0.03	-0.50	0.50	0.11	0.03
250x75x2.5	247.5	197.5	72.5	22.5	2.5	-0.2556	0.03	-0.50	0.50	0.11	0.03
250x60x2.0	248.0	208.0	58.0	18.0	2.0	-0.2556	0.03	-0.50	0.50	0.11	0.03
200x60x2.5	197.5	157.5	57.5	17.5	2.5	-0.2600	0.03	-0.50	0.50	0.11	0.03
200x60x2.0	198.0	158.0	58.0	18.0	2.0	-0.2567	0.03	-0.50	0.50	0.11	0.03
200x45x1.6	198.4	168.4	43.4	13.4	1.6	-0.2567	0.03	-0.50	0.50	0.11	0.03
150x45x2.0	148.0	118.0	43.0	13.0	2.0	-0.2615	0.03	-0.50	0.50	0.11	0.03
150x45x1.6	148.4	118.4	43.4	13.4	1.6	-0.2567	0.03	-0.50	0.50	0.11	0.03
125x45x2.0	123.0	93.0	43.0	13.0	2.0	-0.2615	0.03	-0.50	0.50	0.11	0.03
125x45x1.6	123.4	93.4	43.4	13.4	1.6	-0.2567	0.03	-0.50	0.50	0.11	0.03

Table 3: Comparison of Elastic Buckling Moments of LSBs from FEA, Thin-Wall and Pi and Trahair's [12] Equations

Span (mm)	300x75x2.5 LSB					200x45x1.6 LSB				
	Elastic Buckling Moment			% Difference Compared with FEA		Elastic Buckling Moment			% Difference Compared with FEA	
	FEA	PT	TW	PT	TW	FEA	PT	TW	PT	TW
1000	107.8*	267.3	108.9	-	0.98	25.4*	27.6	25.3	-	-0.16
1500	107.5*	127.6	108.9	-	1.34	15	15.7	15.1	4.69	0.87
2000	78.4	82.4	79	5.16	0.79	11.4	11.8	11.5	3.79	1.14
3000	51.6	53.4	52.1	3.38	0.93	8.3	8.6	8.5	2.91	1.46
4000	41.6	42.7	42.1	2.74	1.18	6.7	6.8	6.8	2.53	1.78
6000	31.1	31.7	31.5	2.20	1.55	4.7	4.8	4.8	2.11	2.07
8000	24.7	25.2	25.2	1.95	1.78	3.7	3.7	3.7	1.94	2.22
10000	20.4	20.8	20.8	1.81	1.91	3	3	3	1.80	2.23

* Subject to local buckling, TW – Thin-Wall, PT – Pi and Trahair's [12] Equations.

Table 4: Comparison of Experimental and FEA Ultimate Moment Capacities

Test No	LSB Section	Span (mm)	Yield Stress, f_y (MPa)			Ult. Moment Capacity (kNm)		EXP/ FEA
			Outside flange	Inside Flange	Web	EXP	FEA	
1	250x75x2.5 LSB*	3500	552.2	502.2	446.0	34.13	36.90	0.92
2	300x60x2.0 LSB*	4000	557.7	496.3	447.1	17.17	17.80	0.96
3	200x45x1.6 LSB*	4000	536.9	491.3	456.6	5.92	6.23	0.95
4	300x60x2.0 LSB*	3000	557.7	496.3	447.1	18.09	18.40	0.98
5	200x45x1.6 LSB	3000	536.9	491.3	456.6	9.24	8.92	1.04
6	150x45x1.6 LSB	3000	557.8	487.5	455.1	8.27	8.28	1.00
7	150x45x2.0 LSB	3000	537.6	491.8	437.1	9.87	10.50	0.94
8	200x45x1.6 LSB	2000	536.9	491.3	456.6	10.72	10.10	1.06
9	150x45x2.0 LSB	2000	537.6	491.8	437.1	10.76	11.20	0.96
10	150x45x1.6 LSB	1800	557.8	487.5	455.1	9.30	9.00	1.03
11	125x45x2.0 LSB	1200	544.1	493.4	444.4	10.83	10.40	1.04

*Tests without stiffener plates at the supports

Table 5: Comparison of Moment Capacities from FEA and AS/NZS 4600 [21]

LSB Section	Span	M_{od}	M_y	λ_d	FEA	M_u / M_y		Ratio
	(mm)	(kNm)	(kNm)		M_u (kNm)	FEA	AS/NZS 4600	FEA/ AS/NZS 4600
300x75x3.0 LSB	2000	97.87	77.24	0.89	54.52	0.71	0.66	1.06
	4000	52.37	77.24	1.21	40.92	0.53	0.49	1.09
	6000	38.00	77.24	1.43	32.45	0.42	0.41	1.02
	8000	29.71	77.24	1.61	26.6	0.34	0.37	0.94
	10000	24.29	77.24	1.78	22.55	0.29	0.31	0.93*
250x75x3.0 LSB	2000	89.72	60.06	0.82	48.24	0.8	0.72	1.11
	4000	51.78	60.06	1.08	39.41	0.66	0.55	1.20
	6000	37.46	60.06	1.27	31.97	0.53	0.47	1.14
	8000	29.14	60.06	1.44	26.4	0.44	0.41	1.07
	10000	23.75	60.06	1.59	22.49	0.37	0.37	1.01
200x60x2.0 LSB	2000	29.57	25.79	0.93	18.54	0.72	0.63	1.14
	4000	18.13	25.79	1.19	14.75	0.57	0.49	1.16
	6000	13.19	25.79	1.4	11.79	0.46	0.42	1.08
	8000	10.27	25.79	1.58	9.71	0.38	0.37	1.01
	10000	8.37	25.79	1.75	8.29	0.32	0.32	0.99*
150x45x2.0 LSB	2000	14.52	14.35	0.99	10.23	0.71	0.59	1.20
	4000	8.17	14.35	1.33	7.13	0.5	0.45	1.12
	6000	5.62	14.35	1.6	5.36	0.37	0.37	1.01
	8000	4.26	14.35	1.83	4.37	0.3	0.3	1.02*

*outside the inelastic lateral buckling region (elastic buckling region)

Table 6: Capacity Reduction Factors for Eq.7

Results	Mean, P_m	COV, V_p	Φ
FEA / Eq.7 (b)	1.02	0.066	0.92
EXP / Eq.7 (b)	0.98	0.105	0.86
(FEA + EXP) / Eq.7 (b)	1.01	0.080	0.90